

ISSN 0257-9731

# JOURNAL OF THE CHINESE SOCIETY OF MECHANICAL ENGINEERS



VOL. 15 NO. 1  
February 1994

Transactions of the Chinese Institute  
of Engineers, Series C

中國工程師學會學刊系列 C

## 中國機械工程學刊

Published by the Chinese Society of Mechanical Engineers

Taipei, Taiwan, Republic of China.

# Journal of the Chinese Society of Mechanical Engineers

February, 1994

Vol.15, No.1

## CONTENTS

### Papers

- |   |  |    |
|---|--|----|
| Finite Element Modeling of Heat Transfer and Residual Stress Analysis<br>for Electron Beam Welding .....                          | Ming-Chang Jeng and Cheng-Tang Wu              | 1  |
| Analysis of Asymmetrical Cold Strip Rolling by Force<br>Equilibrium Method .....  | Gow-Yi Tzou and Yeong-Maw Hwang                | 11 |
| Effect of Aging Treatment on the Fatigue and Mechanical Properties<br>of T-250 Maraging Steel .....                               | Leu-Wen Tsay, Chun Chen and Jong-Ning Aoh      | 23 |
| The Effect of Distributed or Discrete Pressure and Acceleration<br>Sensors on Active Structural-Acoustic Control Systems<br>..... | Bor-Tsuen Wang and Chris R. Fuller             | 30 |
| Disturbance Propagation and Design of Power Transmission<br>Reduction in an L-type Truss Beam .....                               | Rong-Tyai Wang                                 | 40 |
| An Approach for Reducing the Peak Acceleration of Cam-Follower<br>Systems Using a B-Spline Representation ...                     | Hong-Sen Yan and Ming-Kwo Fong                 | 48 |
| Flow Calculation in a Loop-Scavenged Direct-Injection Two-<br>Stroke Engine .....   | Yeng-Yung Tsui, Po-Jung Chen and Shinn-Juen Yu | 56 |

### Research Notes

- |  |                                  |    |
|--|----------------------------------|----|
| Hydrodynamic Characteristics of a Confined Slot Jet<br>Impingement ..... | Yuh-June Chou and Ying-Huei Hung | 71 |
| Axisymmetric Buckling of Thick Polar Orthotropic Annular<br>Plates ..... | Jeng-Shian Chang                 | 79 |
| Vibration Analysis of a Multi-Span Beam .....                            | Rong-Tyai Wang                   | 88 |

# The Effect of Distributed or Discrete Pressure and Acceleration Sensors on Active Structural-Acoustic Control Systems

Bor-Tsuen Wang\* and Chris R. Fuller\*\*

Keywords: adaptive feedforward control, cost function, structural acoustics, wavenumber, radiation efficiency.

## ABSTRACT

This paper presents four types of cost functions, which are based on the use of distributed or discrete pressure and acceleration sensors, for structural sound radiation control in conjunction with the use of the LMS control algorithm. In order to study the influence of cost functions, a system consists of baffled simply-supported plate radiating into a half space is analytically considered. The disturbance input is a harmonic point force, while control is applied by piezoelectric actuators bonded to the structure. The error sensors are either accelerometers, microphones or distributed sensors. To compare the control effectiveness and mechanism of these cost functions, excitation on-resonance and off-resonance was considered. Both the radiation directivity pattern and plate displacement distribution were obtained as well as the average radiation efficiency and radiated power. Additionally, plate wavenumber analysis is also discussed. This work shows that distributed sensors generally perform better than discrete sensors, and pressure sensors are shown to have considerable advantages over acceleration sensors in structural sound radiation control.

## INTRODUCTION

Active noise control has been increasingly used and shown to be effective in attenuating low-frequency sound. The LMS adaptive feedforward control approach has also been successfully applied to active structural-acoustic control (ASAC) (Burgess, 1981; Elliott et al., 1987; Erikson et al., 1987). To construct a LMS adaptive controller, a quadratic cost

function is generally formulated as the error criterion. Quadratic optimization theory is then applied to minimize the cost function so as to adjust control signals to actuators in order to attenuate the structural sound radiation due to a noise input. The total radiated power is usually chosen as the cost function for theoretical formulations (Fuller, 1988; Dimitriadis and Fuller, 1989; Wang et al., 1990). Although this type of cost function indicates the highest possible attenuation, the total radiated power is not measurable in practice. Fuller et al. (1989) proposed the use of discrete microphones in the radiation far-field as well as accelerometers mounted on the vibrating structure surfaces to serve as error sensors. They experimentally demonstrated the performance of both types of error sensors for active control of sound transmission through an elastic plate by applying vibrational forces directly to the structure. Error microphones in the radiated field which provide acoustic information were shown to be generally advantageous over error accelerometers on the plate.

This paper presents four types of cost functions, which are based on the use of distributed or discrete pressure and acceleration sensors, for ASAC in conjunction with the use of the LMS adaptive control algorithm. In order to study the influence of cost functions, a system consisting of baffled simply-supported plate radiating into a half space is analytically considered. The disturbance input is a harmonic point force, while control is applied by piezoelectric actuators bonded to the structure. The error sensors are either accelerometers, microphones or distributed sensors. To compare the control effectiveness and mechanism inherent in these cost functions, excitation on-resonance and off-resonance was considered. Both the radiation directivity pattern and plate displacement distribution were obtained as well as the average radiation efficiency and radiated power. Additionally, plate wavenumber analysis is also discussed. This

Paper Received October, 1991. Accepted December, 1993. Author for Correspondence: B. T. Wang.

\* Associate Professor, Department of Mechanical Engineering, National Pingtung Polytechnic Institute, Pingtung, Taiwan, ROC.

\*\* Professor, Department of Mechanical Engineering, Virginia Polytechnic Institute and State University, Virginia, USA.

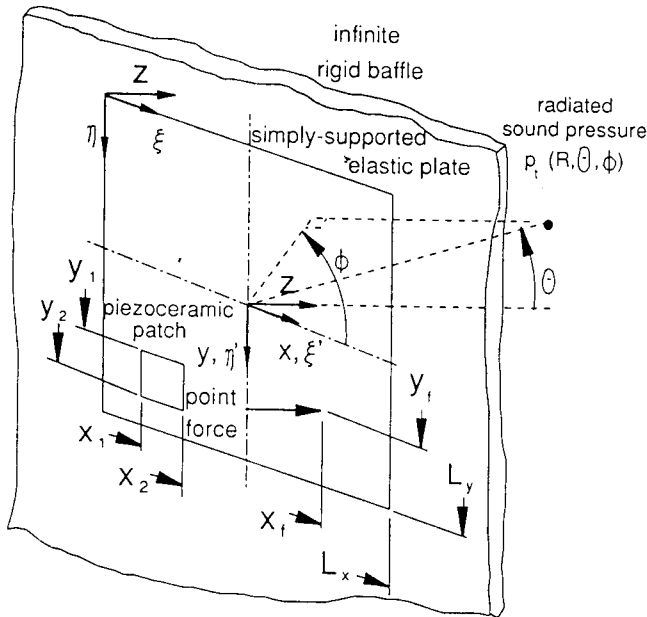


Fig.1. Arrangement and coordinates of the system.

work shows that distributed sensors generally perform better than discrete sensors, and pressure sensors are shown to have considerable advantages over acceleration sensors in ASAC.

## THEORETICAL ANALYSIS

### Plate Vibration for Noise and Control Inputs

Figure 1 shows the arrangement and coordinates of the system. Point forces considered as noise sources were used to excite the plate, and piezoelectric actuators considered as control sources were applied to control the plate sound radiation. Under the assumption of harmonic excitation, the displacement of the simply-supported plate can be written as:

$$w(\xi, \eta, t) = e^{j\omega t} \sum_{m=1}^{\infty} \sum_{n=1}^{\infty} W_{mn} \sin\left(\frac{m\pi}{L_x}\xi\right) \sin\left(\frac{n\pi}{L_y}\eta\right), \quad (1)$$

where  $W_{mn} = P_{mn}/\rho_p h(\omega_{mn}^2 - \omega^2)$ ,  $\omega_{mn}$  are natural frequencies,  $\rho_p$  is the plate density,  $h$  the plate thickness, and  $P_{mn}$  the modal force which depends on the exact description of the applied external load. The expressions of modal forces corresponding to point force and piezoceramic actuator inputs are given in Wang (1991).

### Sound Radiation

The radiated sound pressure can be evaluated from the Rayleigh integral which relates the plate velocity to the transmitted pressure. An approximate closed-form solution for this integral can be obtained in the far-field (Junger and Feit, 1986; Rousos, 1985). For  $N_s$  noise sources (point forces) or  $N_c$  piezoelectric actuators, the sound pressure radiated to a point,  $p(R, \theta, \phi)$ , in the far-field for light fluid loading can be derived as follow:

Noise sources:

$$p_n(R, \theta, \phi) = K \sum_{j=1}^{N_s} \sum_{m=1}^{\infty} \sum_{n=1}^{\infty} W_{mnj}^f I_m I_n, \quad (2)$$

Control sources:

$$p_c(R, \theta, \phi) = K \sum_{j=1}^{N_c} \sum_{m=1}^{\infty} \sum_{n=1}^{\infty} W_{mnj}^c I_m I_n, \quad (3)$$

where the constant  $K$  and the quantities  $I_m$  and  $I_n$  can be found in Roussos (1985) as functions of  $(R, \theta, \phi)$ . When the noise sources and the piezoelectric actuators act simultaneously, the total sound pressure field can be viewed as a superposition of the above given sound pressures for steady-state harmonic excitation (i.e.,  $p_t = p_n + p_c$ ).

### Cost Function

The possible candidates of the cost function used in sound radiation control corresponding to different types of sensors can be as follows:

Distributed pressure sensors:

$$\Phi_p = \int_s |p_t|^2 R^2 \sin \theta d\theta d\phi, \quad (4)$$

Discrete pressure sensors:

$$\Psi_p = \sum_{i=1}^{N_{mike}} |p_{t_i}(R_i, \theta_i, \phi_i)|^2, \quad (5)$$

Distributed acceleration sensors:

$$\Phi_w = \int_A |\dot{w}_t|^2 dA = \int_0^{L_y} \int_0^{L_x} |\dot{w}_t|^2 dx dy, \quad (6)$$

Discrete acceleration sensors:

$$\Psi_w = \sum_{i=1}^{N_{acc}} |\dot{w}_t(x_i, y_i)|^2. \quad (7)$$

The above cost functions are positive definite quadratic functions. Linear quadratic optimization control theory (Lester and Fuller, 1990) can be applied to determine the optimal control voltage inputs to actuators so as to minimize a specified cost function. The detailed derivation given in (Wang, 1991) will not be shown here for brevity. It is noted that  $\Phi_p$  and  $\Phi_w$  are measured by ideal distributed sensors, which may not be practical in reality; however,  $\Phi_p$  and  $\Phi_w$  represent the power of sound radiated or energy density of out-of-plane structural vibration. They can be used as an index of control effectiveness. For practical applications,  $\Psi_p$  and  $\Psi_w$ , the alternative options, are for microphones in the radiated far-field and accelerometers on the vibrating structure surface respectively.

### Plate Wavenumber Analysis

The plate velocity distribution,  $\dot{w}(\xi', \eta')$ , can be derived from Eq.(1) and transformed to the central origin plate coordinates  $(\xi', \eta')$ . The wavenumber transform of plate velocity is then given by Fahy (1985)

$$\tilde{V}(\kappa_x, \kappa_y) = \int_{-L_y/2}^{L_y/2} \int_{-L_x/2}^{L_x/2} \dot{w}(\xi', \eta') e^{-j(\kappa_x \xi' + \kappa_y \eta')} d\xi' d\eta'. \quad (8)$$

The radiated power has been shown in Fahy (1985) to be related to the integration of the modulus square of  $\tilde{V}(\kappa_x, \kappa_y)$ . Therefore, it is of interest to evaluate the wavenumber modulus spectrum of plate velocity,  $|\tilde{V}(\kappa_x, \kappa_y)|^2$ .

### Mode Radiation Efficiency

The radiation efficiency of the  $(m, n)$  mode is defined as (Wallace, 1972):

$$\sigma_{mn} = \frac{\Pi_{mn}}{\rho c L_x L_y \langle |\bar{u}| \rangle^2} = \frac{8\Pi_{mn}}{\rho c L_x L_y \omega^2 W_{mn}^2}, \quad (9)$$

where  $\Pi_{mn}$  is the radiated power due to the  $(m, n)$  mode response, and  $\langle |\bar{u}| \rangle^2$  is the temporal and spatial average of the square of the  $(m, n)$  mode plate velocity. Note that  $\sigma_{mn}$  represents the radiation efficiency of the  $(m, n)$  mode and can be considered as a structural-acoustic property which indicates the acoustic coupling between mechanical vibration and sound radiation.

### Average Radiation Efficiency

Similar to definition of the  $(m, n)$  mode radiation efficiency, the average radiation efficiency can also be defined as (Berry et al., 1990):

$$\sigma = \frac{\Pi}{\rho c L_x L_y \langle |\bar{u}| \rangle^2} = \frac{8\Pi}{\rho c L_x L_y \omega^2 \sum_{m=1}^{\infty} \sum_{n=1}^{\infty} W_{mn}^2}, \quad (10)$$

where  $\Pi$  is the total power radiated from the plate, and  $\langle |\bar{u}| \rangle^2$  is the temporal and spatial average of the square of the plate velocity. The average radiation efficiency indicates the overall acoustic coupling between the mechanical vibration and sound radiation for the plate subjected to a specific noise input. The two summations of  $m$  and  $n$ , as shown in Eq.(10), include the cross product between modes which are significant and cannot be ignored.

### ANALYTICAL RESULTS

Numerical examples presented are based on a steel plate with length of 380mm, width of 300mm and thickness of 2mm. The plate natural frequencies are tabulated in Table 1. For simplicity, a single harmonic point force of amplitude  $F = 1N$  located at  $x_f = 0.316m$ ,  $y_f = 0.15m$  was used as the noise disturbance. Likewise, a single control piezoelectric actuator of thickness  $t_a = 0.1905mm$  with a piezoelectric strain coefficient of  $d_{31} = 166 \times 10^{-12}m/V$  was employed, located at  $x_1 = 0.158m$ ,  $x_2 = 0.222m$ ,

Table 1. Natural frequency of simply supported plate (Hz).

| m\n | 1      | 2       | 3       | 4       | 5       |
|-----|--------|---------|---------|---------|---------|
| 1   | 87.71  | 249.81  | 519.98  | 898.22  | 1384.53 |
| 2   | 188.74 | 350.85  | 621.02  | 999.25  | 1485.56 |
| 3   | 357.13 | 519.23  | 789.40  | 1167.64 | 1653.95 |
| 4   | 592.88 | 754.98  | 1025.15 | 1403.39 | 1889.69 |
| 5   | 895.98 | 1058.08 | 1328.25 | 1706.48 | 2192.79 |

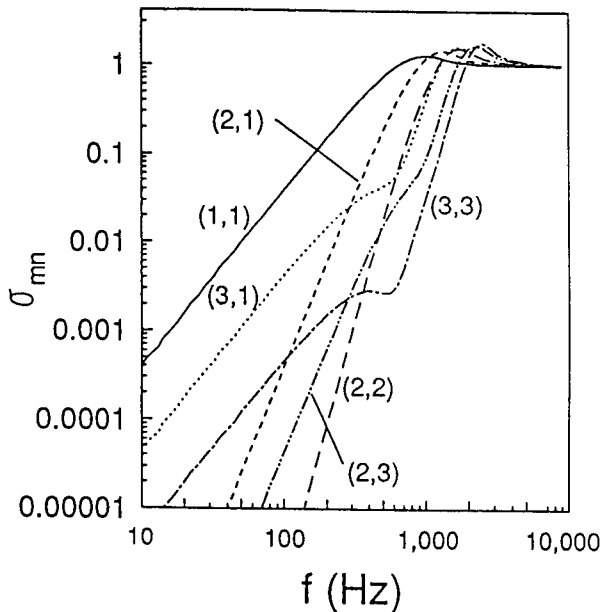


Fig.2. Radiation efficiency vs. frequency.

$y_1 = 0.130m$ ,  $y_2 = 0.170m$ . When a single error sensor was used, a microphone at  $(R, \theta, \phi) = (1.8m, 0^\circ, 0^\circ)$  in the far-field or an accelerometer at  $(x, y) = (0.19m, 0.15m)$  on the plate is considered.

### Radiation Efficiency of the $(m, n)$ Mode

Figure 2 shows the  $(m, n)$  mode radiation efficiency for the plate under consideration plotted against the excitation frequency. The  $(1, 1)$ ,  $(3, 1)$  and  $(3, 3)$  modes, (the odd-odd modes), have higher radiation efficiencies than the  $(2, 1)$ ,  $(2, 3)$ , (the odd-even and even-odd modes), and the  $(2, 2)$  modes, (the even-even mode). This indicates that the odd-odd modes are the effective radiating modes with strongly acoustic coupling between sound radiation and mechanical vibration, and the even-even modes, subjected to radiation cancellation, have smaller radiation efficiencies. When the excitation frequency is greater than the modal critical frequency, the radi-

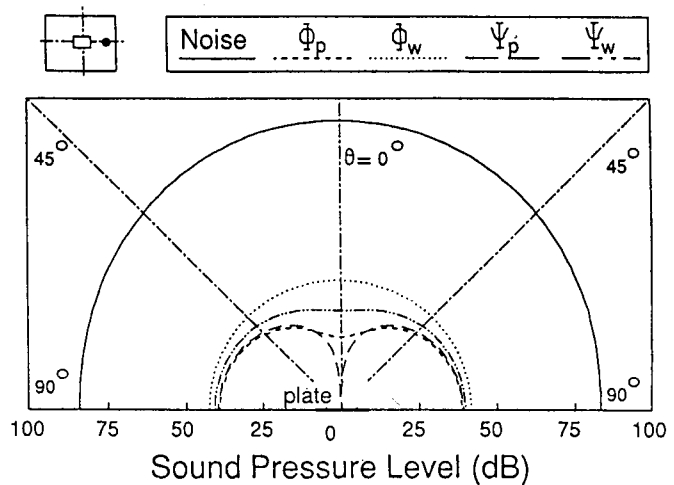


Fig.3. Radiation directivity pattern,  $f = 357Hz$ .

ation efficiencies approach asymptotically to unity. The surprising observation from Fig.2 is that the  $(2, 1)$  mode radiation efficiency is greater than the  $(3, 1)$  mode radiation efficiency between  $300Hz$  and  $1000Hz$  which is within our study range ( $357Hz$  for the  $(3, 1)$  resonance mode). The  $(2, 1)$  mode, previously thought to be a less effective radiator, actually has significant contribution.

### On-Resonance Excitation

Figure 3 shows the radiation directivity of the noise with a excitation frequency of  $357Hz$  near the  $(3, 1)$  mode resonance point. The system arrangement is sketched on the top of Fig.3. The noise radiation directivity, denoted by a solid line, can be seen to be fairly constant with radiation angle. This behavior is due to the relatively long wavelength of the acoustic radiation relative to plate size, leading to the higher order plate  $(3, 1)$  mode giving a radiating field which is volumetric or monopole like.

If the distributed pressure sensors over a hemisphere of radiating field are used, the corresponding cost function  $(\Phi_p)$  can be constructed as defined in Eq.(4). The sound pressure level can be thus reduced globally over the radiating field as it is observed at all angles. The residual radiation directivity exhibits a combination of the  $(1, 1)$  and  $(2, 1)$  mode responses. If a discrete pressure sensor (the corresponding cost function,  $\Psi_p$ , defined in Eq.(5)) is used and located at  $(R, \theta, \phi) = (1.8m, 0^\circ, 0^\circ)$ , the residual radiation directivity reveals a dipole response, because the sound pressure at the location of the error microphone is reduced to zero. Similarly, a distributed or discrete acceleration sensor, located at  $(x, y) = (0.19m, 0.15m)$ ,

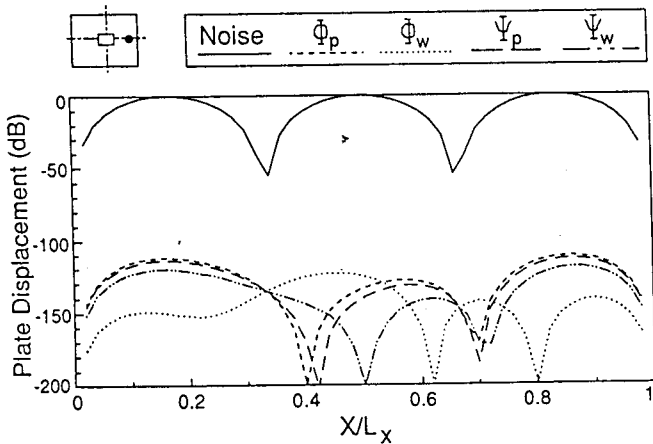


Fig.4. Plate displacement distribution,  $f = 357\text{Hz}$ .

can be used, and the cost functions are then defined in Eqs. (6) ( $\Phi_w$ ) and (7) ( $\Psi_w$ ) respectively. The residual radiation directivity for these two cost functions exhibits a monopole or a distorted monopole response. Generally, for on resonance, any one of the cost functions results in a global reduction of the far-field sound radiation; however, there are slight differences between the residual radiation pattern for different forms of cost functions. These subtle differences reveal important insights into the different control mechanisms associated with each form of the cost function; and these effects are enhanced for off-resonance control. The results again show that the pressure sensor is superior to the acceleration sensor in sound radiation control as discussed by Fuller et al. (1989), because the pressure sensor supplies the coupling information between sound radiation and mechanical vibration while the acceleration sensor supply only the information of mechanical vibration. In other words, the pressure sensor directly measures the variable(s) to be minimized.

Figure 4 shows the plate displacement distribution corresponding to the case of Fig.3. The plate displacement distribution is plotted along the  $y = L_y/2$  horizontal plate midline. The results are normalized by the largest amplitude obtained in each case. As expected, the (3, 1) mode dominates the plate vibration due to the noise input frequency being near the (3, 1) resonance point. With control, the plate response is attenuated globally for all cost functions and exhibits a slightly complex pattern. As observed, the residual plate response for  $\Phi_w$  is generally the lowest, and there is a zero response at  $x/L_x = 0.5$  for  $\Psi_w$  because of the central location of the accelerometer. Note that using accelerometer sensors will result in more attenuation of plate displacement than using pressure sensors; however, the corresponding sound

Table 2. Summary of on-resonance excitation case.

| On-resonance excitation, $f = 357\text{ Hz}$ |                           |                              |                                |                                  |
|--|---------------------------|------------------------------|--------------------------------|----------------------------------|
| cost function form                           | control voltages V(volts) | average radiation efficiency | reduction of cost function(dB) | reduction of radiated power (dB) |
| Disturbance                                  |                           | 0.03366                      |                                |                                  |
| $\Phi_p$                                     | 24.958                    | 0.00449                      | 57.46                          | 57.46                            |
| $\Phi_w$                                     | 25.037                    | 0.11336                      | 54.56                          | 49.28                            |
| $\Psi_p$                                     | 24.967                    | 0.00566                      | 144.03                         | 57.18                            |
| $\Psi_w$                                     | 24.990                    | 0.01584                      | 153.81                         | 54.74                            |

pressure levels are not generally attenuated to the degree that the plate displacement is attenuated.

Table 2 shows the applied voltage to the piezoelectric actuator and the reduction of cost function and radiated power as well as the average radiation efficiency, when different forms of cost functions were used. The distributed pressure sensor is the most effective giving the most reduction of radiated power and the lowest average radiation efficiency. All four cost functions have nearly the same control voltages. Both the distributed and discrete pressure sensors have about the same reduction of radiated power, and generally perform better than the acceleration sensors, either distributed or discrete.

Figures 5(a) and 5(b) show the plate wavenumber spectrum along axis  $\kappa_x$  and  $\kappa_y$  respectively, and only the positive components  $\kappa_x$  and  $\kappa_y$  are shown for brevity. The spectrum of the noise field is denoted by a solid line shown in Fig.5(a). A peak near values of  $\kappa_x = 3\pi/L_x$  and  $\kappa_y = 0$  indicates that the plate response is dominated by the (3, 1) mode. Figure 5(a) also indicates that there is a substantial spectral component at  $\kappa_x = 0$ , i.e., the (1, 1) mode is significant in the plate response. The spectral content of the controlled response can be seen to be strongly reduced at all wavenumbers for all of the cost functions. This indicates that the plate response has globally fallen explaining the overall drop in the plate response in Fig.4. Also shown on the plots of Figs. 5(a) and 5(b) is the acoustic wavenumbers,  $\kappa = \omega/c = 6.54\text{m}^{-1}$ . As is well known, only supersonic wavenumber components (i.e.,  $(\kappa_x^2 + \kappa_y^2)^{-1/2} < \kappa$ ) radiate sound to the far-field. When control is applied, all supersonic wavenumber components are seen to be reduced, corresponding to global control of sound radiation. When a discrete pressure sensor is used, the wavenumber components around  $\kappa_x, \kappa_y = 0$  are observed to be strongly attenuated, corresponding to a high local reduction in sound at the error microphone.

Another interesting observation from Fig.5 is

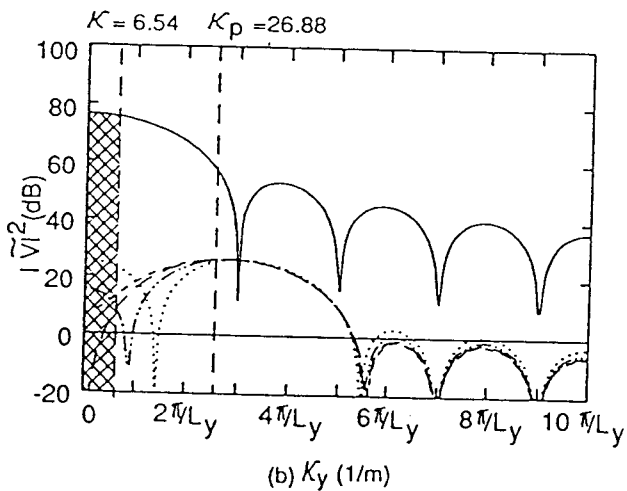
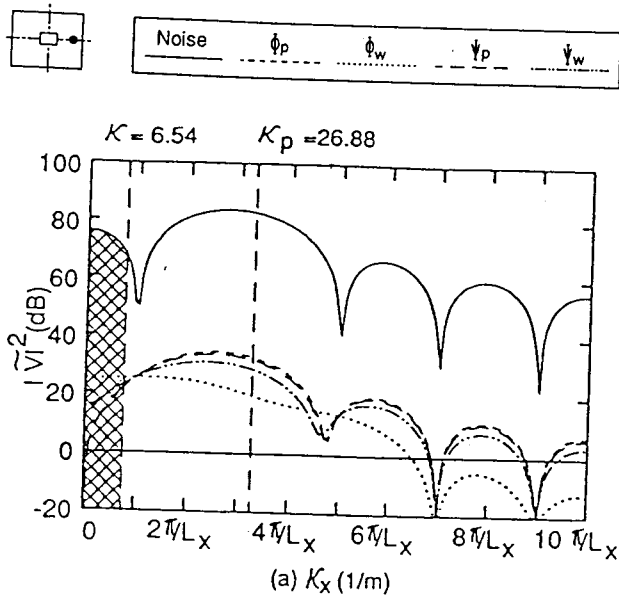


Fig.5. Wavenumber spectra of plate velocity,  $f = 357\text{Hz}$ .

that the oscillations in the spectral distributions at low wavenumbers has been smoothed. This indicates that the residual plate-baffle response is dominated by high wavenumber components or short wavelength, higher modal order motion. Thus two control mechanisms are observed. The first, termed "modal suppression" (Fuller et al., 1991), implies that the plate response falls globally and corresponds to a fall in wavenumber components across the complete spectrum. The second, termed "modal restructuring" (Fuller et al., 1991), implies that the plate residual response becomes more complex (higher modal order) with a lower radiation efficiency. Conversely "modal restructuring" corresponds to a decrease in the supersonic wavenumber components while the subsonic components remain unchanged or even increase. Such

Table 3. Summary of off-resonance excitation case.

| Off-resonance excitation, $f = 272\text{ Hz}$ |                           |                              |                                |                                  |
|---|---------------------------|------------------------------|--------------------------------|----------------------------------|
| cost function form                            | control voltages V(volts) | average radiation efficiency | reduction of cost function(dB) | reduction of radiated power (dB) |
| Disturbance                                   |                           | 0.01275                      |                                |                                  |
| $\Phi_p$                                      | 6.3449                    | 0.00885                      | 0.82                           | 0.82                             |
| $\Phi_w$                                      | 16.573                    | 0.04977                      | 1.03                           | -4.88                            |
| $\Psi_p$                                      | 4.7574                    | 0.00938                      | 152.85                         | 0.77                             |
| $\Psi_w$                                      | 17.572                    | 0.05296                      | 153.63                         | -5.16                            |

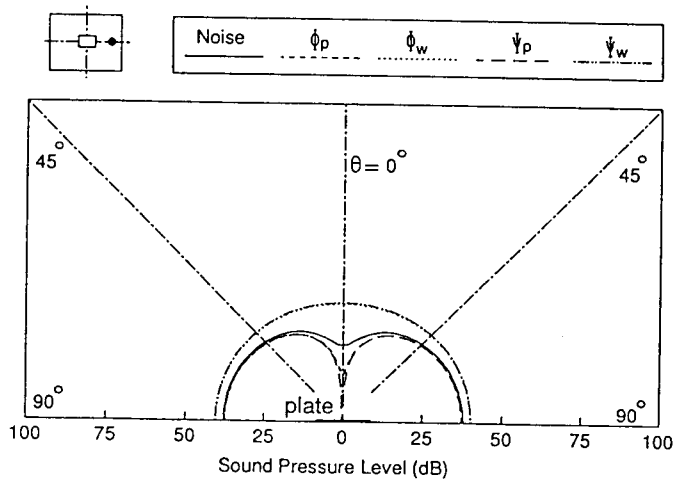


Fig.6. Radiation directivity pattern,  $f = 272\text{Hz}$ .

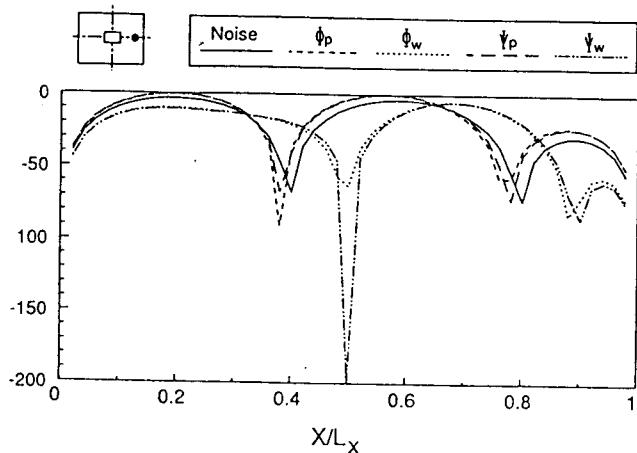


Fig.7. Plate displacement distribution,  $f = 272\text{Hz}$ .



behavior has also been observed in companion experiments (Clark and Fuller, 1990), and is shown to be enhanced for off-resonance conditions (Wang, 1991).

**Off-Resonance Excitation**

Figure 6 shows the radiation directivity of the disturbance with an excitation frequency of  $272\text{Hz}$  between the (2, 1) and (3, 1) modes, controlled by one piezoelectric actuator as sketched on the top of Fig.6. The primary sound radiation directivity is denoted by a solid line, and can be seen to have a small dip at  $\theta = 0^\circ$ . This indicates that the primary sound radiation directivity is contributed significantly by the (1, 1) and (2, 1) modes. The reduction of radiated power is only  $0.82\text{dB}$  and  $0.77\text{dB}$  for distributed and discrete pressure sensors respectively. In the case of using pressure sensors, the discrete sensor has about the same residual response as the distributed except at  $\theta = 0^\circ$ , where the sound pressure is reduced to zero, because of the location of the discrete pressure sensor. Only a small amount of reduction of sound pressure level can be achieved. In the case of using acceleration sensors, the residual radiation directivity reveals spillover to the sound pressure in the far-field. Although the plate vibration energy density or vibrational levels have been reduced (i.e., the reduction of cost function  $\Phi_w$  or  $\Psi_w$ , which is referenced to  $10^{-12}\text{W/m}^2$ ), as observed in Table 3, the total reduction of radiated power is negative for acceleration sensors, i.e., the radiation field shows spillover. The control voltages required by acceleration sensors is higher than those by pressure sensors.

Figure 7 shows the displacement distribution corresponding to the cases of Fig.6. In contrast to the radiation directivity shown in Fig.6, in which the (1, 1) and (2, 1) modes dominates the sound radiation to the far-field, the plate response is dominated by the (3, 1) mode. As shown in Fig.2, the (1, 1) and (2, 1) modes have higher radiation efficiency than the (3, 1) at  $f = 272\text{Hz}$ ; therefore, the (1, 1) and (2, 1) modes become the dominant radiating modes rather than the (3, 1) mode. When pressure sensors are used, the plate residual displacement distribution is close to the (3, 1) mode, but slightly distorted, and only attenuated a little. Thus control has achieved only  $0.82\text{dB}$  of power reduction as shown in Table 3. This is because the central location of piezoelectric actuator cannot excite the (2, 1) mode which is one of the dominant radiating modes. In the case of using acceleration sensors, the plate response was attenuated, and the (3, 1) modal contribution has been cut down while the (1, 1) and (2, 1) modes become dominant. This leads to the spillover in the radiat-

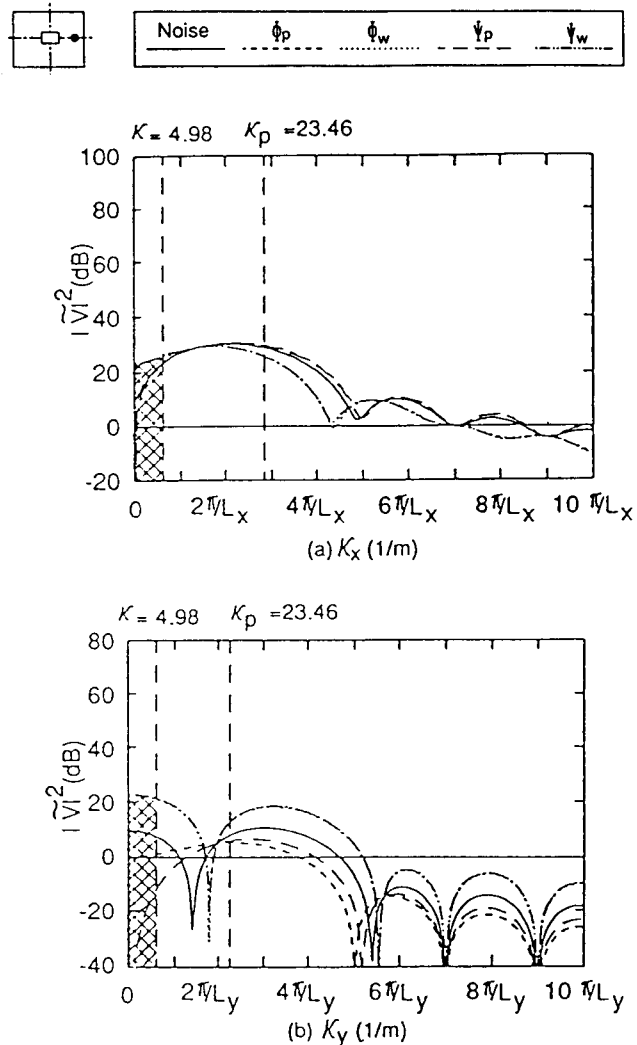


Fig.8. Wavenumber spectra of plate velocity,  $f = 272\text{Hz}$ .

ing field and a monopole like response, because the (1, 1) and (2, 1) modes have higher radiation efficiencies. These results demonstrate a very important effect. Attenuating plate motion does not necessarily lead to reduction in radiated sound. In fact, for off-resonance cases, the inverse is often true with radiated sound levels increasing, while overall plate response decrease.

Figures 8(a) and 8(b) show the plate wavenumber spectrum along axis  $\kappa_x$  and  $\kappa_y$  respectively corresponding to the cases of Figs. 6 and 7. From Fig.8(a), the primary field reveals a maximum between  $2\pi/L_x$  and  $3\pi/L_x$  near the  $\kappa_p = 23.29\text{m}^{-1}$ , for this off-resonance excitation of  $f = 272\text{Hz}$ , and the spectra become smooth for supersonic waves. The acoustic wavenumber ( $\kappa = 4.98\text{m}^{-1}$ ) is also marked as a dash line in Figs. 8(a) and 8(b). As

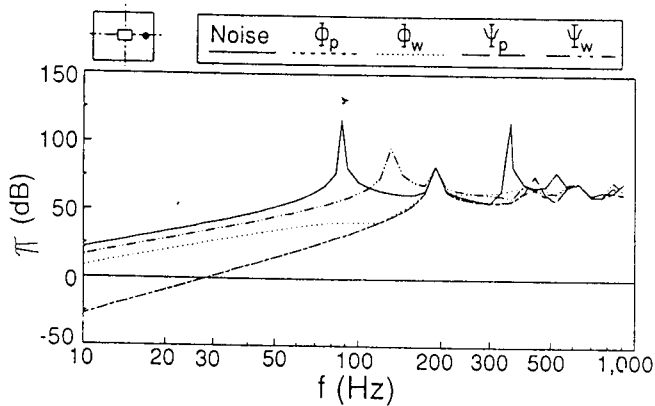


Fig.9. Radiated power vs. frequency.

discussed previously, above this line the wavenumber components recognized as subsonic waves do not contribute to the sound radiation; however, supersonic waves, i.e., wavenumber components below the acoustic wavenumber, do radiate to the far-field. In the case of using pressure sensors, the supersonic components have been reduced while the subsonic components were increased. This results in a small amount of radiated power reduction as shown in Table 3, and the phenomenon is termed "modal restructuring", i.e., the plate vibration pattern becomes close to the (3, 1) mode, as seen in Fig.7. In other words, the significant radiation modes have been changed to less efficient mode radiators due to the change of plate vibration pattern, and this change, thus, leads to a reduction of radiated power. In particular, the wavenumber spectrum equals to zero at  $\kappa_x = \kappa_y = 0$  (where  $\kappa_x = \kappa \cos \theta \sin \phi$  and  $\kappa_y = \kappa \sin \theta \sin \phi$ ), with the discrete pressure sensor located at  $(1.8m, 0^\circ, 0^\circ)$ . When the pressure is minimized in the far-field at a particular angle, the corresponding wavenumber component to that angle is suppressed. In the case of using acceleration sensors, the subsonic components have been reduced while the supersonic components were increased. The increase at  $\kappa_x = \kappa_y = 0$  especially indicates spillover of control energy into the (1, 1) mode. This explains why the residual radiation directivity reveals a monopole response in the case of using acceleration sensors as shown in Fig.6. Figure 8(b) shows the similar plot along the  $\kappa_y$  axis. The disturbance denoted by a solid line reveals a  $n = 1$  dominant mode pattern, i.e., the (3, 1) mode. Again, the analysis of wavenumber spectra also demonstrates that pressure sensors perform better than acceleration sensors. In effect, the distributed far-field pressure sensor acts as distributed structural-wavenumber sensor. They observe every radiating point on the

plate and also every supersonic wavenumber component while not observing the subsonic components.

### Cost Function Performance Versus Frequency

Figure 9 shows the radiated power for the noise with and without control plotted against the excitation frequency for different forms of cost functions corresponding to the previous case. The solid line denotes the noise and reveals several peaks, such as at 87, 190, 357, 520 and 620 Hz, which are near the natural frequencies of the simply-supported plate. In the case of using pressure sensors, both discrete and distributed sensors have about the same residual radiated power, and a large amount of power reduction is achieved below 180 Hz near the (2, 1) mode. For higher frequency excitation, since more high modal responses contribute to the sound radiation, only a slight reduction can be achieved for using just one actuator. Additionally, there is no improvement at excitation of the even modes, such as the (2, 1), (2, 2), (4, 1) and (4, 2) modes, because of the central location of the piezoelectric actuator. Of course, attenuation could be achieved with multiple, appropriately located actuators as shown previously (Wang et al., 1990).

In the case of using acceleration sensors, the radiated power has been attenuated at low frequency range, but the reduction is not as much as that using pressure sensors. The distributed acceleration sensor, located over the plate, generally performs better than the discrete acceleration sensor, located at the center of the plate. For the discrete acceleration sensor, the radiated power increases between 105 and 190 Hz, i.e., between the (1, 1) and (2, 1) modes, while the radiated power decreases for other selection of sensors. This is because the accelerometer cannot effectively observe the plate response at the central location in this range of excitation frequency, where the (2, 1) mode dominates the plate response. The residual radiated power in the case of using distributed acceleration sensors is close to that of using pressure sensors between 110 and 190 Hz, but is higher at frequencies below 110 Hz. This can be explained by the observation that controlling the (1, 1) plate modal response is not effective in the reduction of sound radiation within this range. However, controlling the (2, 1) plate modal response is effective since the (2, 1) mode is the dominant radiator to radiated field in this frequency band.

Figure 10 shows the average radiation efficiency plotted against the frequency corresponding to the cases of Fig.9. The average radiation efficiency generally agrees with the radiated power because of the

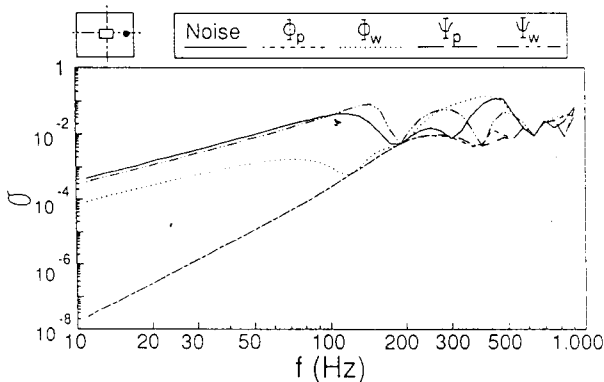


Fig.10. Average radiation efficiency vs. frequency.

coupling relation as shown in Eq.(10). The noise denoted by a solid line reveals no peaks, unlike what was observed in Fig.9 for radiated power. In the case of using pressure sensors, average radiation efficiency generally decreases, except where the control is not achievable, such as 190 and 280Hz. In the case of using acceleration sensors, the average radiation efficiency increases over some frequency ranges where the overall acoustic coupling was intensified.

## CONCLUSIONS

This paper evaluates the control effectiveness and control mechanism for different forms of cost functions used in the feedforward quadratic optimal control approach applied to ASAC. The cost functions are constructed based on the use of either distributed or discrete pressure and acceleration sensors, with one piezoelectric actuator as the control input. Numerical examples illustrate the role of modal radiation efficiency which is associated with the structural-acoustic coupling properties and is independent of the nature of disturbance. The average radiation efficiency, which is associated with the sum of all of modal distributions and is thus dependent on the nature of disturbance, represents acoustic coupling between the sound radiation and the residual mechanical vibration. Wavenumber domain analysis is also discussed and shown to be a very powerful tool providing an alternative view of ASAC.

Results also showed that distributed sensors which can reveal global system response generally perform better than discrete sensors which can only provide a few point responses; however, in practice, a finite number of discrete sensors can only be used. In term of the reduction of radiated power over a frequency range, pressure sensors are superior to acceleration sensors, because pressure sensors inherently

supply the structural-acoustic coupling information while acceleration sensors can only provide the mechanical vibration information. The proposed control strategy can be applied to obtain the optimal location of actuators and sensors and to design near-field pressure sensors with the effect of minimizing the far-field pressure.

## REFERENCES

- Berry, A., Guyada, J.-L., and Nicolas, J. "A General Formulation for the Sound Radiation from Rectangular, Baffled Plates with Arbitrary Boundary Conditions," *Journal of the Acoustical Society of American*, Vol.88, No.6, pp.2792-2803 (1990).
- Burgess, J. C., "Active Adaptive Sound Control in a duct: A Computer Simulation," *Journal of Acoustical Society of American*, Vol.70, No.3, pp.715-726 (1981).
- Clark, R. L., and Fuller, C. R., "An Experimental Study of the Use of PVDF Piezoelectric Sensors in Active Structural Acoustic Approaches," *Journal of the Acoustical Society of American*, Vol.88(s1), p. s 148 (1990).
- Dimitriadis, E. K., and Fuller, C. R., "Investigation on Active Control of Sound Transmission Through Elastic Plates Using Piezoelectric Actuators," *AIAA-89-1062* (1989).
- Elliott, S. J., Stothers, I. M., and Nelson, P. A., "A Multiple Error LMS Algorithm and its Application to the Active Control of Sound and Vibration," *IEEE Transactions on Acoustics, Speech, and Signal Processing*, Vol.ASSP-35, No.10, pp.1423-1434 (1987).
- Eriksson, L. J., Allie, M. C., and Greiner, R. A., "The Selection and Application of an IIR Adaptive Filter for Use in Active Sound Attenuation," *IEEE Transactions on Acoustics, Speech, and Signal Processing*, Vol.ASSP-35, No.4, pp.433-437 (1987).
- Fahy, F., *Sound and Structural Vibration: Radiation, Transmission and Response*, Academic Press, Inc., Orlando, Florida (1985).
- Fuller, C. R., "Analysis of Active Control of Sound Radiation from Elastic Plates by Force Inputs," *Proceedings of Inter-Noise 88*, pp.1061-1064 (1988).
- Fuller, C. R., Silcox, R. J., Metcalf, V. L., and Brown, D. E., "Experiments on Structural Control of Sound Transmitted Through an Elastic Plate," *Proceedings of the American Control Conference*, pp.2079-2084 (1989).

- Fuller, C. R., Hansen, C. H., and Snyder, S. D., "Active Control of Sound Radiation From a Vibrating Rectangular Panel by Sound Sources and Vibration Inputs: an Experimental Comparison," *Journal of Sound and Vibration*, Vol.14, No.2, pp.195-215 (1991).
- Junger, M. C., and Feit, D., *Sound, Structures and their Interaction*, 2nd ed., MIT press, Cambridge, MA (1986).
- Lester, H. C., and Fuller, C. R., "Active Control of Propeller Induced Noise Fields Inside a Flexible Cylinder," *AIAA Journal*, Vol.28, No.8, pp.1374-1380 (1990).
- Roussos, L. A., "Noise Transmission Loss of a Rectangular Plate in an Infinite Baffle," *NASA Technical Paper 2398* (1985).
- Wallace, C. E., "Radiation Resistance of a Rectangular Panel," *Journal of Acoustical Society of American*, Vol.51, pp.946-952 (1972).
- Wang, B.-T., Dimitriadis, E. K., and Fuller, C. R., "Active Control of Structurally Radiated Noise Using Multiple Piezoelectric Actuators," *Proceedings of the AIAA/ASME/ASCE/AHS 31st Structures, Structural Dynamics and Materials Conference*, Long Beach, CA, AIAA-90-1172 (1990).
- Wang, B.T., "Active Control of Sound Transmission/Radiation from Elastic Plates Using Multiple Piezoelectric Actuators," PhD Dissertation, VPI & SU, Blacksburg, Virginia, (1991).

## 均佈或零散之聲壓及加速度感應器在主動結構噪音控制系統之效應

王栢村\* Chris R. Fuller\*\*

\* 國立屏東技術學院機械工程技術系  
\*\* 美國維州理工暨州立大學機械系

### 摘要

此篇報告提出四種型態的成本函數用於結構聲音幅射控制，配合最小平方自調式控制法，此成本函數乃基於所使用之均佈或零散的壓力或加速度感應器而定，為研究成本函數的影響，以一阻隔之簡支板的聲音幅射做理論性之分析，以協振點力為干擾源，而以壓電驅動器黏貼在結構上做為控制源，誤差感應器則用加速度感應器，麥克風，或者均佈式感應器。為比較各成本函數的控制效果及其控制形態，激振於共振點和非共振點都同時考慮，而得到聲音幅射方向型譜，板位移分佈，平均聲音幅射效率和聲音幅射能。另外板波數分析也同時探討。此篇報告證明，在結構聲音幅射控制中，均佈感應器通常優於零散感應器，而壓力感應器也有相當程度地優於加速度感應器。